PROCEEDINGS OF SCIENCE

Analysis of T_{cc}^+ including chiral dynamics and three-body cuts

Meng-Lin Du,[a,*] **Vadim Baru,**[b,c] **Xiang-Kun Dong,**[d,e] **Arseniy Filin,**[b] **Feng-Kun Guo,**[d,e] **Christoph Hanhart,**[f] **Alexey Nefediev,**[g] **Juan Nieves**[a] **and Qian Wang**[h,i,j]

[a] *Instituto de Física Corpuscular (centro mixto CSIC-UV), Institutos de Investigación de Paterna, Apartado 22085, 46071, Valencia, Spain*

[b] *Institut für Theoretische Physik II, Ruhr-Universität Bochum, D-44780 Bochum, Germany*

[c] *Institute for Theoretical and Experimental Physics NRC "Kurchatov Institute", Moscow 117218, Russia*

[d] *CAS Key Laboratory of Theoretical Physics, Institute of Theoretical Physics, Chinese Academy of Sciences, Beijing 100190, China*

[e] *School of Physical Sciences, University of Chinese Academy of Sciences, Beijing 100049, China*

[f] *Institute for Advanced Simulation, Institut für Kernphysik and Jülich Center for Hadron Physics, Forschungszentrum Jülich, D-52425 Jülich, Germany*

[g] *P.N. Lebedev Physical Institute of the Russian Academy of Sciences, 119991, Leninskiy Prospect 53, Moscow, Russia*

[h] *Guangdong Provincial Key Laboratory of Nuclear Science, Institute of Quantum Matter, South China Normal University, Guangzhou 510006, China*

[i] *Institute of High Energy Physics, Chinese Academy of Sciences, Beijing 100049, China*

[j] *Guangdong-Hong Kong Joint Laboratory of Quantum Matter, Southern Nuclear Science Computing Center, South China Normal University, Guangzhou 510006, China*

E-mail: du.menglin@ific.uv.es, vadim.baru@tp2.rub.de, dongxiangkun@itp.ac.cn, arseniy.filin@ruhr-uni-bochum.de, fkguo@itp.ac.cn, c.hanhart@fz-juelich.de, nefediev@lebedev.ru, jmnieves@ific.uv.es, qianwang@m.scnu.edu.cn

A coupled-channel approach is applied to the charged tetraquark state T_{cc}^+ with special attention paid to the three-body dynamics. The three-body unitarity is preserved as both the pion exchange between the D and D^* mesons and the finite D^* width are taken into account simultaneously. The low-energy scattering parameters, namely the scattering length and effective range are extracted with a low-energy expansion of the D^*D scattering amplitude. The compositeness parameter is calculated and is found to be close to unity, which implies a molecular nature of the T_{cc}^+. By making use of the heavy-quark spin symmetry, an isoscalar D^*D^* molecular partner of the T_{cc}^+ with $J^P = 1^+$ is predicted under the assumption that the D^*D-D^*D^* coupled-channel effects can be neglected.

The 10th International Workshop on Chiral Dynamics - CD2021
15-19 November 2021
Online

*Speaker

PoS(CD2021)051

1. Introduction

Recently, the LHCb Collaboration discovered a double-charm exotic structure T_{cc}^+ just below the $D^{*+}D^0$ threshold in the $D^0D^0\pi^+$ invariant mass distribution [1, 2]. The parameters of the resonance extracted from a generic constant-width Breit-Wigner fit built by LHCb in Ref. [1] are

$$\begin{aligned}\delta m_{\rm BW} &= -273 \pm 61 \pm 5^{+11}_{-14}\ \text{keV},\\ \Gamma_{\rm BW} &= 410 \pm 165 \pm 43^{+18}_{-38}\ \text{keV},\end{aligned}$$

where $\delta m_{\rm BW}$ defines the mass with respect to the $D^{*+}D^0$ threshold. Since approximately 90% of the $D^0D^0\pi^+$ events contain a genuine D^{*+} meson [2], it is natural to expect the width of the T_{cc}^+ to be smaller than that of the D^{*+}, which is only (83.4 ± 1.8) keV [3]. A more profound analysis, based on a unitarized and analytical model, is performed by LHCb in Ref. [2]. The extracted pole is located in the complex energy plane at [2]

$$\sqrt{s}_{\rm pole} = \left[-360 \pm 40^{+4}_{-0} - i\,(24 \pm 1^{+0}_{-7})\right]\ \text{keV}, \tag{1}$$

with respect to the $D^{*+}D^0$ threshold. The imaginary part of the pole, corresponding to the half width of the T_{cc}^+, is in agreement with the natural expectation. While the value of the scattering length is found to be well constrained, i.e. $a = [-(7.16 \pm 0.51) + i(1.85 \pm 0.58)]$ fm, the effective range r is consistent with zero and only an upper limit on $-r$ is provided [2],

$$0 \leqslant -r < 11.9\,(16.9)\ \text{fm at 90 (95)\% CL}. \tag{2}$$

The Weinberg compositeness criterion [4, 5] making use of the relation between the scattering length and the effective range generates an upper limit of the compositeness parameter Z,

$$Z < 0.52\,(0.58)\ \text{at 90 (95)\% CL}, \tag{3}$$

for which $Z = 1$ corresponds to a compact state that does not interact with the continuum while $Z = 0$ indicates a composite state formed by hadronic interactions. It implies that the properties of the T_{cc}^+ are consistent with a molecular nature. In addition, due to the proximity of the T_{cc}^+ to the $D^{*+}D^0$ threshold and a small energy release in the $D^{*+} \to D^0\pi^+$ decay, a narrow peak just above the D^0D^0 (and D^+D^0) threshold is formed in the D^0D^0 (D^+D^0) mass distribution. Nevertheless, neither the $D^+D^0\pi^+$ nor D^+D^+ mass distribution exhibit any narrow peaking structure, which indicates that the T_{cc}^+ is an isoscalar state.

The discovery of the T_{cc}^+ quickly spurred numerous phenomenological studies, see e.g. Refs. [6–9]. In this talk, we investigate the properties of the T_{cc}^+ in the framework of a nonrelativistic effective field theory constrained with the chiral and heavy-quark spin symmetries. It is noted that the static approximation for the one-pion-exchange (OPE) in the charmonium/double-charm systems of interest is not justified since the three-body intermediate state involving the exchanged pion can go on shell. The three-body effects are expected to have a strong impact on the properties of the T_{cc}^+ due to the proximity of the three-body threshold to the T_{cc}^+. Therefore we proceed beyond the simplest approach based solely on the short-range interactions (see e.g. Ref. [10]) and include the long-range OPE interactions in a nonperturbative way. A study of the behavior of the scattering amplitude for

the coupled-channel system and unstable components in the vicinity of the $D^{*+}D^0$ threshold results in the proper determination of the low-energy scattering parameters and the compositeness of the T_{cc}^+. The $D^{(*)}D^{(*)}$ interactions are independent of the heavy-quark spin according to HQSS, which is employed to predict the existence of a D^*D^* molecular state T_{cc}^{*+}, as a HQSS partner of the T_{cc}^+. More details con be found in Refs. [18, 20].

2. Framework

2.1 Interaction potentials

The proximity of the T_{cc}^+ to the D^*D thresholds suggests that the dominating component is a S-wave D^*D pair. The quantum numbers of such a system, $J^P = 1^+$, perfectly match the observation of the LHCb Collaboration [1, 2]. The isoscalar ($I = 0$) and isovector ($I = 1$) combinations can be constructed as

$$|D^*D, I = 0\rangle = -\frac{1}{\sqrt{2}}(D^{*+}D^0 - D^{*0}D^+), \quad |D^*D, I = 1\rangle = -\frac{1}{\sqrt{2}}(D^{*+}D^0 + D^{*0}D^+). \tag{4}$$

The leading order (LO) $D^{(*)}D^{(*)}$ contact interaction in the chiral effective field theory contains only $O(p^0)$ contact potentials, with p a soft momentum scale [11],

$$\begin{aligned}\mathcal{L}_{HH} = &-\frac{D_{10}}{8}\mathrm{Tr}\left(\tau^A_{aa'}H^\dagger_{a'}H_b\tau^A_{bb'}H^\dagger_{b'}H_a\right) - \frac{D_{11}}{8}\mathrm{Tr}\left(\tau^A_{aa'}\sigma^i H^\dagger_{a'}H_b\tau^A_{bb'}\sigma^i H^\dagger_{b'}H_a\right)\\ &-\frac{D_{00}}{8}\mathrm{Tr}\left(H^\dagger_a H_b H^\dagger_b H_a\right) - \frac{D_{01}}{8}\mathrm{Tr}\left(\sigma^i H^\dagger_a H_b \sigma^i H^\dagger_b H_a\right),\end{aligned} \tag{5}$$

where the subscripts $a^{(\prime)}$, $b^{(\prime)}$ are flavor indices, $\tau^{A=1,2,3}$ denote the isospin Pauli matrices, and the $D_{00,10,01,11}$ are low-energy constants (LECs). The heavy-light mesons grouped into a superfield,

$$H_a = P_a + \vec{V}_a \cdot \vec{\sigma}, \tag{6}$$

with P_a and $\vec{V}_a$ annihilating the ground-state pseudoscalar and vector charmed mesons, respectively,

$$D^{(*)} = \begin{pmatrix} D^{(*)0} \\ D^{(*)+} \end{pmatrix}. \tag{7}$$

The S-wave contact potentials can be derived from the Lagrangian (5),

$$V_{\rm CT}^{I=0}(D^*D \to D^*D; J^P = 1^+) = -2(D_{01} - 3D_{11}) \equiv v_0, \tag{8}$$

$$V_{\rm CT}^{I=1}(D^*D \to D^*D; J^P = 1^+) = D_{00} + D_{01} + D_{10} + D_{11} \equiv v_1, \tag{9}$$

where we have introduced the isoscalar and isovector interaction strength v_0 and v_1, respectively. Since the study of the DD mass spectra support an isoscalar interpretation of the T_{cc}^+ [2], in what follows we stick to the isoscalar contact interaction and neglect the isovector one, that is, $v_1 = 0$, to reduce the number of free parameters. Note that the isospin symmetry is assumed for the contact potential while the breaking effects are taken into account explicitly through the mass difference for the charged and neutral $D^{(*)}$'s and pions.

The LO OPE potential can be obtained from the effective Lagrangian for the axial coupling of pions to charmed mesons [12]

$$\mathcal{L} = \frac{1}{4} g \, \mathrm{Tr}\left(\vec{\sigma} \cdot \vec{u}_{ab} H_b H_a^\dagger\right), \tag{10}$$

where $\vec{u} = -\nabla\Phi/f_\pi$ with

$$\Phi = \begin{pmatrix} \pi^0 & \sqrt{2}\pi^+ \\ \sqrt{2}\pi^- & -\pi^0 \end{pmatrix}. \tag{11}$$

Here $f_\pi = 92.1$ MeV is the pion decay constant and the coupling $g = 0.57$ is determined from the experimentally measured $D^{*+} \to D^0\pi^+$ decay width [3]. Once the OPE is considered, both the S and D waves are included as their mixture can have a sizable impact on the line shapes between the thresholds [13–16].

2.2 Lippman-Schwinger equation

One can obtain the $D^{*+}D^0$ production amplitude $U_\alpha(M, p)$ satisfying the three-body unitarity by solving a Lippmann-Schwinger equations (LSEs),

$$U_\alpha(M, p) = P_\alpha - \sum_\beta \int \frac{\mathrm{d}^3\vec{q}}{(2\pi)^3} V_{\alpha\beta}(M, p, q) G_\beta(M, q) U_\beta(M, q), \tag{12}$$

where P_α is the point-like production source with $\alpha = 1(2)$ denoting the $D^{*+}D^0$ ($D^{*0}D^+$) channel. Since we only focus on the isoscalar contact potential, the isopsin symmetry requires that $P_2 = -P_1$ which can then be absorbed by the overall normalization factor.

The three-body cuts give rise to complementary contributions, with a graphical representation shown in Fig. 1. While the three-body cut associated with the OPE is included in the interaction

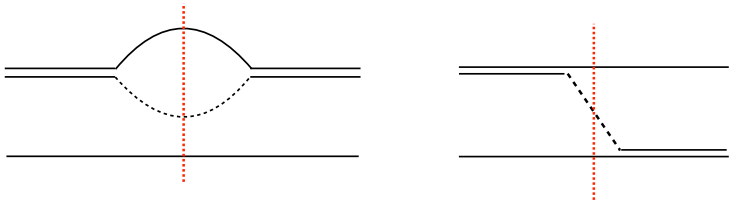

Figure 1: Graphical representation for the three-body cuts (shown with the vertical dotted red lines).

potential $V_{\alpha,\beta}(M, p, q)$ in Eq. (12), the cut associated with the D^* self-energy is encoded in the full D^*D propagators

$$\begin{aligned} G_1(M, p) = G_3(M, p) &= \left[m_c^* + m_0 + \frac{p^2}{2\mu_{c0}} - M - \frac{i}{2}\Gamma_c(M, p)\right]^{-1}, \\ G_2(M, p) = G_4(M, p) &= \left[m_0^* + m_c + \frac{p^2}{2\mu_{0c}} - M - \frac{i}{2}\Gamma_0(M, p)\right]^{-1}, \end{aligned} \tag{13}$$

where the reduced masses are $\mu_{c0} = m_c^* m_0/(m_c^* + m_0)$ and $\mu_{0c} = m_0^* m_c/(m_0^* + m_c)$, and the energy-dependent widths read [17, 18]

$$\begin{aligned}
\Gamma_c(M,p) &= \Gamma(D^{*+} \to D^+\gamma) + \frac{g^2 m_0}{12\pi f_\pi^2 m_c^*}\Sigma_{D^0\pi^+D^0}(M,p,\mu_{c0}) + \frac{g^2 m_c}{24\pi f_\pi^2 m_c^*}\Sigma_{D^+\pi^0D^0}(M,p,\mu_{c0}),\\
\Gamma_0(M,p) &= \Gamma(D^{*0} \to D^0\gamma) + \frac{g^2 m_0}{24\pi f_\pi^2 m_0^*}\Sigma_{D^0\pi^0D^+}(M,p,\mu_{0c})\\
&\quad + \frac{g^2 m_c}{12\pi f_\pi^2 m_0^*}\left[\Sigma_{D^+\pi^-D^+}(M,p,\mu_{0c}) - \Sigma_{D^+\pi^-D^+}(m_c+m_0^*,0,\mu_{0c})\right],
\end{aligned}$$

where

$$\Sigma_{ijk}(M,p,\mu) = \left[2\mu_{ij}\left(M - m_i - m_j - m_k - \frac{p^2}{2\mu}\right)\right]^{3/2}, \tag{14}$$

with $\mu_{ij} = m_i m_j/(m_i + m_j)$. To render the integrals in the LSEs in Eq. (12) well defined we regularize them with a sharp cutoff Λ. We have verified that the physical observables are almost Λ-independent in the range $\Lambda \in [0.3, 1.2]$ GeV. Below we present the numerical results corresponding to $\Lambda = 0.5$ GeV.

3. Data analysis

3.1 Fit to the $D^0D^0\pi^+$ spectrum

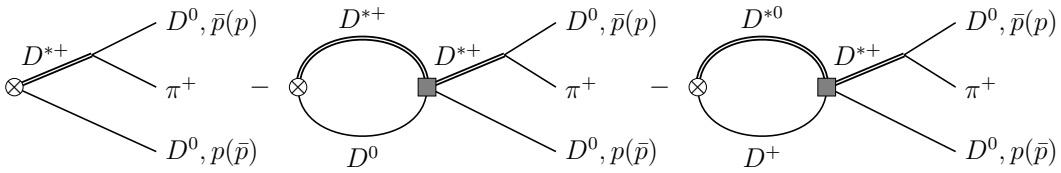

Figure 2: Graphical representation for the production amplitude in the $D^0D^0\pi^+$ channel with the DD^* final state interaction.

The production rate for the three-body $D^0D^0\pi^+$ channel, with a diagrammatic representation shown in Fig. 2, is calculated as [17, 18]

$$\frac{\mathrm{d}\,\mathrm{Br}[D^0D^0\pi^+]}{\mathrm{d}\,M} = \mathcal{N}\int_0^{p_{\max}} p\,\mathrm{d}p \int_{\bar{p}_{\min}}^{\bar{p}_{\max}} \bar{p}\,\mathrm{d}\bar{p}\ \left|q_\pi U_1(M,p)G_1(M,p) + \bar{q}_\pi U_1(M,\bar{p})G_1(M,\bar{p})\right|^2,$$

where $\mathcal{N}$ is a normalization constant,

$$q_\pi = \sqrt{2\mu_{D^0\pi^+}\left(M - 2m_0 - m_{\pi^+} - \frac{p^2}{2\mu_p}\right)}, \quad \bar{q}_\pi = \sqrt{2\mu_{D^0\pi^+}\left(M - 2m_0 - m_{\pi^+} - \frac{\bar{p}^2}{2\mu_p}\right)},$$

and

$$p_{\max} = \sqrt{2\mu_p(M - 2m_0 - m_{\pi^+})}, \quad \bar{p}_{\min,\max} = \left|\sqrt{2\mu_{D^0\pi^+}\left(M - 2m_0 - m_{\pi^+} - \frac{p^2}{2\mu_p}\right)} \mp \frac{m_0 p}{m_0 + m_{\pi^+}}\right|,$$

with $\mu_p = m_0(m_0 + m_{\pi^+})/(2m_0 + m_{\pi^+})$.

In order to assess the role of the three-body effects, we consider three different fit schemes:

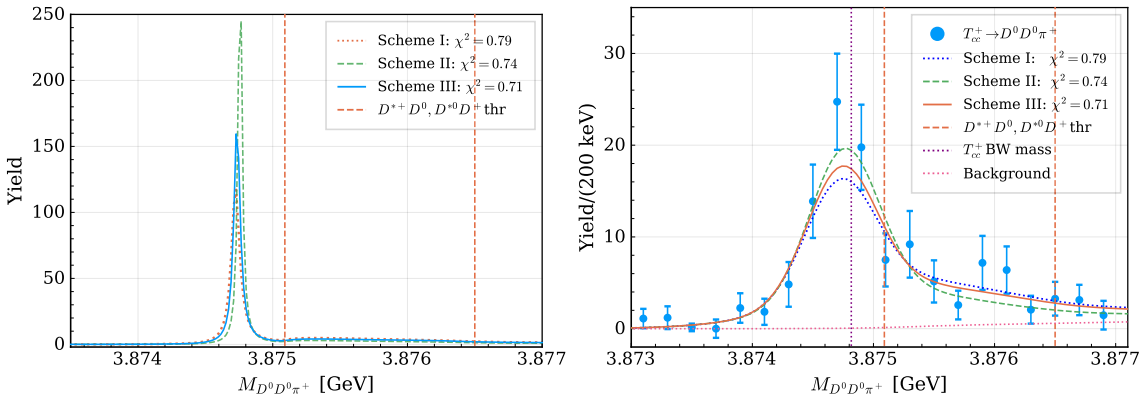

Figure 3: Fitted line shapes before (left) and after (right) convolution with the energy resolution function.

- Scheme I (no three-body effects): only the LO contact potentials are employed with the constant D^* widths, $\Gamma_0(M, p) = 53.7$ keV and $\Gamma_c(M, p) = 82.5$ keV.
- Scheme II (partial three-body effects): the dynamical widths of the D^* mesons are implemented (left diagram in Fig. 1) while the OPE potential is not included (right diagram in Fig. 1).
- Scheme III (full three-body effects): the OPE potentials are added to Scheme II for a complete account for the full three-body effects.

In all schemes above, the background is taken from the LHCb analysis in Refs. [1, 2]. In addition, the detector resolution is modeled by a sum of two Gaussian functions as given in Ref. [2].

The fit results for the three fit schemes are shown in Fig. 3, where the quoted value of χ^2/d.o.f. can be employed to assess the quality of the corresponding fit. The positions of the pole responsible for the T_{cc}^+ in each scheme are collected in Table 1. The real and imaginary parts of the pole are identified with the binding energy and half width of the T_{cc}^+, respectively. In Scheme I, where a constant width of the D^* is employed and hence no three-body cut is involved, the T_{cc}^+ pole is located on the first (physical) Riemann sheet (RS-I), just below the $D^{*+}D^0$ threshold and thus corresponds to a shallow bound state. It is worth mentioning that by including a constant D^* width, one distorts the two-body cut, which does not any longer spread along the real axis, so that the pole on the RS-I below the threshold acquires an imaginary part.

Scheme	I (RS-I)	II (RS-II)	III (RS-II)
Pole [keV]	$-368^{+43}_{-42} - i(37 \pm 0)$	$-333^{+41}_{-36} - i(18 \pm 1)$	$-356^{+39}_{-38} - i(28 \pm 1)$

Table 1: The position of the T_{cc}^+ pole relative to the $D^{*+}D^0$ threshold and the Riemann sheet (RS) where it is located for the three fitting schemes employed (see the text for further details). The errors are statistical, propagated from the uncertainties in the LHCb data, while those from the cutoff variation are well within the uncertainties quoted here.

When the three-body channels are included explicitly in Schemes II and III, the three-body cuts appear with the branch points at the three-body thresholds. In these two schemes, the T_{cc}^+ pole

is located on the lower half plane of the second Riemann Sheet (RS-II) connected to the physical region (upper half plane of RS-I) along the three-body cut. It is instructive to notice that neglecting the three-body dynamics one overestimates the T_{cc}^+ width by up to a factor of 2, which is consistent with the observation obtained in Refs. [16, 17]. By comparing the imaginary parts of the pole positions for Schemes II and III, one can conclude that the OPE contributes around 20 keV into the T_{cc}^+ width.

3.2 Low-energy expansion of the scattering amplitude

The $D^*D \to D^*D$ scattering amplitude can be obtained by solving a coupled-channel LSE,

$$T_{\alpha\gamma}(M,p,p') = V_{\alpha\gamma}(M,p,p') - \sum_\beta \int \frac{\mathrm{d}^3\vec{q}}{(2\pi)^3} V_{\alpha\beta}(M,p,q) G_\beta(M,q) T_{\beta\gamma}(M,q,p'). \tag{15}$$

A study of the behavior of the scattering amplitude in the vicinity of the $D^{*+}D^0$ branch point results in a determination of the low-energy S-wave scattering parameters, that is, the scattering length a_0 and effective range r_0 defined as

$$T_{D^{*+}D^0\to D^{*+}D^0}(k) = -\frac{2\pi}{\mu_{c0}} \left(\frac{1}{a_0} + \frac{1}{2} r_0 k^2 - ik + O(k^4) \right)^{-1}. \tag{16}$$

It is important to notice that a finite D^* width drives the three-momentum k ill-defined in the vicinity of the two-body D^*D threshold with a real D^* mass. In order to get a deeper insight into the effects of the finite D^* width, let us start from a single-channel problem with a constant contact potential v_c which corresponds to a single-channel version of the Scheme I introduced above. Then the inverse amplitude reads

$$T^{-1}(M) = v_c^{-1} + J(M), \quad J(M) = \int \frac{\mathrm{d}^3\vec{p}}{(2\pi)^3} G(M,p). \tag{17}$$

In this trivial example, the effective range $r_0 \propto -\mathfrak{Re} \frac{\mathrm{d}J(M)}{\mathrm{d}M}\Big|_{M=M_{\rm thr}+0^+}$ with $M_{\rm thr}$ for the corresponding two-body threshold. A finite width of the D^*, however, significantly modifies the behavior of the $J(M)$ in the vicinity of the two-body threshold as the sharp cusp is smeared by the D^* width, see Fig. 4. Therefore the effective range expansion around the D^*D threshold has a very small radius of convergence because of the nearby complex D^*D branch point. A way to bypass this problem is to employ a complex D^* mass in the relation between the energy and momentum k,

$$M = m_c^* - i\Gamma_c/2 + m_0 + \frac{k^2}{2\mu_{c0}}. \tag{18}$$

Then the expansion point $k \to 0$ is equivalent to $M = m_c^* - i\Gamma_c/2 + m_0$ in the complex energy plane, which is the branch point for the two-body unitarity cut on the unphysical RS. In other words, the effective range expansion is defined around the pole of the D^*D two-body Green's function $G(M,p)$. The effective range expansion with the scattering parameters extracted this way are collected in Table 2.

For the coupled-channel approach involving both the $D^{*+}D^0$ and $D^{*0}D^+$ channels, it is shown in Ref. [20] that the largest contribution to the effective range for the T_{cc}^+ originates from the isospin

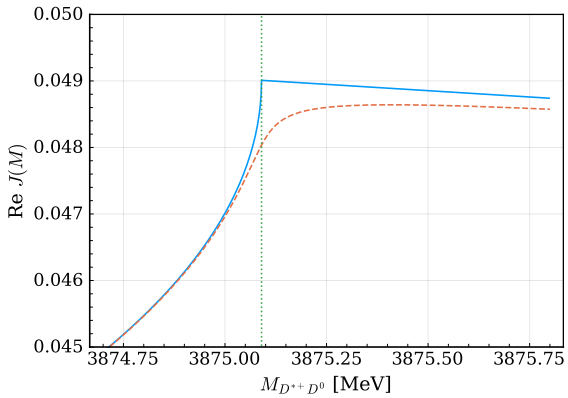

Figure 4: Left: The real part of the single-channel loop function $J(M)$ for a zero (blue solid line) and finite (red dashed line) constant D^{*+} width. The vertical dotted line indicates the $D^{*+}D^0$ threshold.

	$-\frac{\mu_{c0}}{2\pi}T_{\rm thr}$ [fm]	a_0 [fm]	r_0 [fm]	r_0' [fm]	$\bar{X}_A$
I	$\left(-7.38^{+0.46}_{-0.57}\right)+i\left(1.96^{+0.34}_{-0.57}\right)$	$\left(-6.31^{+0.36}_{-0.45}\right)+i\left(0.05^{+0.01}_{-0.01}\right)$	-2.78 ± 0.01	1.00 ± 0.01	0.87 ± 0.01
	± 0.36	± 0.27	± 0.66	± 0.66	± 0.07
		± 0.00			
II	$\left(-8.00^{+0.49}_{-0.68}\right)+i\left(1.88^{+0.36}_{-0.24}\right)$	$\left(-6.64^{+0.36}_{-0.50}\right)-i\left(0.10^{+0.01}_{-0.02}\right)$	-2.80 ± 0.01	0.98 ± 0.01	0.88 ± 0.01
	± 0.35	± 0.27	± 0.59	± 0.59	± 0.06
		± 0.01			
III	$\left(-7.76^{+0.45}_{-0.53}\right)+i\left(2.44^{+0.38}_{-0.29}\right)$	$\left(-6.72^{+0.36}_{-0.45}\right)-i\left(0.10^{+0.03}_{-0.03}\right)$	-2.40 ± 0.01	1.38 ± 0.01	0.84 ± 0.01
	± 0.32	± 0.27	± 0.85	± 0.85	± 0.06
		± 0.03			

Table 2: The scattering length a_0 and 'bare' effective range r_0 defined in Eq. (16), the corrected effective range $r_0' = r_0 - \Delta r_{\rm IB}$ obtained as explained in the text, and the compositeness $\bar{X}_A$ evaluated using Eq. (19). For each quoted value, the error in the first line is statistical, propagated from the LHCb data, while the error in the second line is systematic, from the model uncertainty. The latter is estimated by varying the cutoff parameter Λ in the interval $[0.3, 1.2]$ GeV and taken as the largest deviation from the central value evaluated for $\Lambda = 0.5$ GeV.

breaking (IB) related to the small mass differences between the $D^{*+}D^0$ and $D^{*0}D^+$ channels. This gives rise to $\Delta r_{\rm IB} = -3.78$ fm [20]. By comparing the isospin-violation-corrected effective range $r_0' = r_0 - \Delta r_{\rm IB}$ for Schemes I and II quoted in Table 2, it is found that the residual finite range correction is ≈ 1 fm for $\Lambda = 0.5$ GeV. A comparison of the effective range for Schemes I/II and III indicates the difference ≈ 0.4 fm from the OPE.

The Weinberg compositeness parameter $\bar{X}_A$ can be constructed from the scattering length and effective range as [4, 5]

$$\bar{X}_A = \left(1 + 2\left|\frac{r_0'}{\mathfrak{Re}\, a_0}\right|\right)^{-1/2}, \tag{19}$$

for which $\bar{X}_A \approx 1$ corresponds to a composite state formed by the D^* and D, while $\bar{X}_A \approx 0$ implies

a compact state. The compositenes $\bar{X}_A$ estimated for each scheme is listed in the sixth column of Table 2.

4. Heavy-quark spin symmetry partners of the T_{cc}^+

According to HQSS, the interaction in the D^*D and D^*D^* systems with $J^P = 1^+$ is the same,

$$V^{I=0}(D^*D^* \to D^*D^*, 1^+) = V^{I=0}(D^*D \to D^*D, 1^+). \tag{20}$$

Therefore, the existence of the isoscalar T_{cc}^+ hints at a possible existence of an additional D^*D^* state in the isoscalar $J^P = 1^+$ sector, T_{cc}^{*+}. An accurate prediction of its properties meets certain problems since, as proved in Refs. [13–16], renormalization of the OPE requires inclusion of the next-to-leading order contact interaction to be fixed from experimental data with a nontrivial signal far beyond just the near-threshold region. Furthermore, the D^*D^* two-body propagator contains a four-body cut which is beyond the scope of this work. Nonetheless, as an estimation, we neglect the D^*D-D^*D^* coupled-channel effects and rely on Eq. (20) for the contact potentials. The role of the OPE is assessed by comparing the predictions for the T_{cc}^{*+} pole obtained in different schemes.

We find that while the width of the T_{cc}^+ is sensitive to the D^* width, its mass is stable with respect to different treatments of the D^* width. Therefore, as long as only the mass of the T_{cc}^{*+} is concerned, it is safe to resort to a stable D^*. Then the T_{cc}^{*+} reveals itself as a bound state pole in the isoscalar D^*D^* system with $J^P = 1^+$ and the binding energy $\delta_{cc}^{*+} = m_{T_{cc}^{*+}} - (m_c^* + m_0^*)$,

$$\begin{aligned} &\text{Scheme I:} && \delta_{cc}^{*+} = -1444(61)\ \text{keV}, \\ &\text{Scheme II:} && \delta_{cc}^{*+} = -1138(50)\ \text{keV}, \\ &\text{Scheme III:} && \delta_{cc}^{*+} = -503(40)\ \text{keV}. \end{aligned} \tag{21}$$

A large (~ 1 MeV) spread in the predicted mass of the T_{cc}^{*+} signals a possibly significant role of the OPE.

Acknowledgments

This work is supported in part by the Spanish Ministry of Science and Innovation (MICINN) (Project PID2020-112777GB-I00), by the EU Horizon 2020 research and innovation programme, STRONG-2020 project, under grant agreement No. 824093, by Generalitat Valenciana under contract PROMETEO/2020/023, by the National Natural Science Foundation of China (NSFC) and the Deutsche Forschungsgemeinschaft (DFG) through the funds provided to the Sino-German Collaborative Research Center TRR110 "Symmetries and the Emergence of Structure in QCD" (NSFC Grant No. 12070131001, DFG Project-ID 196253076), by the NSFC under Grants No. 11835015, No. 12047503, No. 11961141012, and No. 12035007, and by the Chinese Academy of Sciences under Grants No. QYZDB-SSW-SYS013, No. XDB34030000, No. XDPB15 and No. 2020VMA0024. The work of A.N. is supported by the Ministry of Science and Education of the Russian Federation under grant 14.W03.31.0026. The work of Q.W. is also supported by Guangdong Major Project of Basic and Applied Basic Research under Grant No. 2020B0301030008, by the Science and Technology Program of Guangzhou under Grant No. 2019050001, and by Guangdong Provincial funding under Grant No. 2019QN01X172.

References

[1] R. Aaij *et al.* [LHCb], [arXiv:2109.01038 [hep-ex]].

[2] R. Aaij *et al.* [LHCb], [arXiv:2109.01056 [hep-ex]].

[3] P. A. Zyla *et al.* [Particle Data Group], PTEP **2020** (2020) no.8, 083C01

[4] S. Weinberg, Phys. Rev. **137** (1965), B672-B678

[5] I. Matuschek, V. Baru, F. K. Guo and C. Hanhart, Eur. Phys. J. A **57** (2021) no.3, 101 [arXiv:2007.05329 [hep-ph]].

[6] L. Meng, G. J. Wang, B. Wang and S. L. Zhu, Phys. Rev. D **104** (2021) no.5, 051502

[7] A. Feijoo, W. H. Liang and E. Oset, Phys. Rev. D **104** (2021) no.11, 114015

[8] M. J. Yan and M. P. Valderrama, Phys. Rev. D **105** (2022) no.1, 014007

[9] S. Fleming, R. Hodges and T. Mehen, Phys. Rev. D **104** (2021) no.11, 116010

[10] M. Albaladejo, [arXiv:2110.02944 [hep-ph]].

[11] T. Mehen and J. W. Powell, Phys. Rev. D **84** (2011), 114013

[12] T. M. Yan, H. Y. Cheng, C. Y. Cheung, G. L. Lin, Y. C. Lin and H. L. Yu, Phys. Rev. D **46** (1992), 1148-1164 [erratum: Phys. Rev. D **55** (1997), 5851]

[13] Q. Wang, V. Baru, A. A. Filin, C. Hanhart, A. V. Nefediev and J. L. Wynen, Phys. Rev. D **98** (2018) no.7, 074023

[14] V. Baru, E. Epelbaum, A. A. Filin, C. Hanhart, A. V. Nefediev and Q. Wang, Phys. Rev. D **99** (2019) no.9, 094013

[15] M. L. Du, V. Baru, F. K. Guo, C. Hanhart, U. G. Meißner, J. A. Oller and Q. Wang, Phys. Rev. Lett. **124** (2020) no.7, 072001

[16] M. L. Du, V. Baru, F. K. Guo, C. Hanhart, U. G. Meißner, J. A. Oller and Q. Wang, JHEP **08** (2021), 157

[17] V. Baru, A. A. Filin, C. Hanhart, Y. S. Kalashnikova, A. E. Kudryavtsev and A. V. Nefediev, Phys. Rev. D **84** (2011), 074029

[18] M. L. Du, V. Baru, X. K. Dong, A. Filin, F. K. Guo, C. Hanhart, A. Nefediev, J. Nieves and Q. Wang, Phys. Rev. D **105** (2022) no.1, 014024

[19] M. Doring, C. Hanhart, F. Huang, S. Krewald and U. G. Meissner, Nucl. Phys. A **829** (2009), 170-209

[20] V. Baru, X. K. Dong, M. L. Du, A. Filin, F. K. Guo, C. Hanhart, A. Nefediev, J. Nieves and Q. Wang, [arXiv:2110.07484 [hep-ph]].